Multiple Internal Reflectance Infrared Spectra of Variably Hydrated Hemoglobin and Myoglobin Films: Effects of Globin Hydration on Ligand Conformer Dynamics and Reactivity at the Heme†

William E. Brown III,‡ Jack W. Sutcliffe, and Phillip D. Pulsinelli*

ABSTRACT: Multiple internal reflectance infrared (IR) spectra are reported for variably hydrated films (1.2–0.1 g of H_2O/g of protein) of the carbon monoxy and oxy forms of human Hb and sperm whale Mb. The spectra show that even the limited removal of liquid and icelike hydration constraints at the globin surface is sufficient to cause a dramatic, but completely reversible, shift toward a normally minute population of sterically unhindered, linear–perpendicular, Fe–CO conformer modes (ν_{CO} = 1968–1967 cm^{-1}), and the destabilization of distally hindered, tilted (or bent), Fe–CO modes (ν_{CO} = 1951, 1944–1933 cm^{-1}). Corroborative evidence from IR band broadening trends [$\Delta\Delta\ \nu_{1/2}$ (1968, 1967 cm^{-1}) ~ 2–4 cm^{-1}], corresponding changes in the visible, and H–D exchange kinetics confirm that the shift toward 1968–1967 cm^{-1} results in a more open distal heme pocket configuration and that it is also accompanied by a buildup of deoxy-like steric hindrance proximal to the heme. Denaturation effects are eliminated as a potential cause of the shifts, as are specific protein–protein, ion–protein, intersubunit, and MIR crystal-film surface interactions. The hydration effect exhibits globin-dependent and ligand-dependent differences, which highlight the intrinsic importance of distal steric effects within the heme pocket and their dynamic coupling with exterior solvent constraints. CO-photodissociation and O_2-exchange experiments conducted on rapidly interconverting (coupled and fully hydrated) and noninterconverting (uncoupled and partially hydrated) Fe–CO conformers also suggest that the open linear–perpendicular mode corresponds to a more tightly bound form of CO than the axially distorted Fe–CO species; similar differences are not evident in $Fe–O_2$, which already prefers a bent end-on geometry within the heme pocket. Control IR spectra aimed at monitoring the progressive effects of various denaturants on HbCO further indicate that this same open mode serves as a common precursor to any of a number of more highly disordered folding modes. The overall properties of the 1968–1967-cm^{-1} conformer are discussed in terms of (1) the possibility of its corresponding to an available relaxation mode capable of facilitating the dynamics of ligand entry–release events and (2) its potential additional significance as a native folding mode that exhibits a marked tendency to be destabilized by hydration.

The aqueous milieu that normally supports, hydrates, and stabilizes the three-dimensional structures of macromolecules is also expected to significantly affect their capacity to change structure, bind ligands, and generally function in a dynamic sense. In Hb[1] and Mb, the surrounding hydration sheath has already been shown to influence the dynamics of ligand transport by forming a surface energy barrier for the entry and release of heme ligands (Austin et al., 1975). This external barrier differs for CO and O_2 trajectories, and it appears to be coupled in a complex dynamic fashion with additional nonequivalent barriers for ligand movements within the heme pocket. Conformational relaxation events occurring throughout the globin framework are thought to form the basis of this coupling.

Theoretical energy minimization treatments of ligand binding dynamics in Hb and Mb lend further support for its close relationship with globin relaxation (Case & Karplus, 1979). Such calculations indicate that both the liganded and unliganded (deoxy) forms of these proteins must undergo some form of dynamic relaxation, if CO and O_2 are to enter or leave the heme pocket at all.[2] The motions of side-chain residues located just distal to the heme (e.g., His-E7 and Val-E11) appear to be directly involved in forming a major part of the stereochemical basis of this relaxation requirement.[2] In addition, these same residues appear to comprise part of a close-packed steric topography, which energetically favors the preferred bent end-on bonding of $Fe–O_2$, while tending to oppose, distort, and weaken the preferred linear–perpendicular configuration of Fe–CO (Case & Karplus, 1978; Collman et al., 1976). The emerging dynamic picture therefore suggests that conformational relaxation should facilitate coupling between the surface constraints afforded by water and internal distal constraints (bonded and nonbonded) that directly affect the bonding and conformer dynamics of heme-bound ligands. Indeed, it would seem that even small perturbations of globin hydration in Hb and Mb should occasionally result in the transmission of globin-dependent and ligand-dependent dynamic effects to the hemes.

We have applied MIR film sampling procedures (Deutschmann & Ullrich, 1979) and a combination of IR and visible spectroscopy to the problem of determining the extent and nature of these interactions. Variably hydrated films were

† From the Department of Medicinal Chemistry, School of Pharmacy, University of Pittsburgh, Pittsburgh, Pennsylvania 15261. *Received October 11, 1982.* This work was supported in part by grants from the National Institutes of Health (AM 18065) and the American Heart Association (77 1072).

‡ Present address: Abbott Laboratories, North Chicago, IL 60064.

[1] Abbreviations: MIR, multiple internal reflectance; IR, infrared; Hb, hemoglobin; Mb, myoglobin; HbCO, (carbon monoxy)hemoglobin; MbCO, (carbon monoxy)myoglobin; HbO_2, oxyhemoglobin; MbO_2, oxymyoglobin; Tris, tris(hydroxymethyl)aminomethane; EDTA, ethylenediaminetetraacetate; BSA, bovine serum albumin; $NaDodSO_4$, sodium dodecyl sulfate.

[2] The energy minimization calculations of Case & Karplus (1979) indicate that ~100 kcal/mol of activation energy would be required for diatomic ligands to leave or enter the heme pocket, if His-E7, Val-E11, and other distal residues are held fixed in their crystallographic atomic model positions. If these same residues are permitted to undergo small relaxational displacements, during ligand entry or release, then trajectory pathways to the globin surface are generated that reduce this barrier to ~5–15 kcal/mol, which is more in accord with kinetically determined values (Austin et al., 1975).

0006-2960/83/0422-2914$01.50/0

chosen for this purpose, because they both minimize undesirable background absorption due to water and provide an effective means of controlling and measuring the extent of hydration. When used in conjunction with measurements of the vibrational stretching of heme-bound CO and O_2, they further provide a means of directly probing any solvent-induced dynamic effects that might be transmitted to the immediate ligand environment. We have also found that film conditions can be established at sufficiently low hydration levels to cause the complete uncoupling of conformational relaxation and, hence, the uncoupling of rapid interconversions between discrete conformer modes. This, in turn, has permitted us to begin to unmask some of the exchange and dissociation properties of individual conformers in the absence of rapid relaxational and equilibrium effects.

Experimental Procedures

Materials. Freshly donated human blood was obtained from the Pittsburgh Central Blood Bank and was worked up to an initial hemolysate within 1 day (Rossi Fanelli et al., 1961). Sperm whale Mb was purchased as the pure ferric powder from Sigma.

Purification and O_2–CO Conversions. Minor Hbs and red cell organic phosphates were removed from hemolysates by DEAE-cellulose chromatography (0.05 M Tris, 10^{-4} M EDTA, pH 7.6). The purified HbO_2 (~2% met-Hb) was concentrated by ultrafiltration to 12–16 mM heme/L for immediate use in the IR or for subsequent conversions to HbCO. Conversions were accomplished by exposing HbO_2 in a glass tonometer to five or more cycles of a water aspirator vacuum followed by positive atmospheres of pure CO.

Ferrous MbO_2 was made by first dissolving 3 g (1.76×10^{-4} mol) of the ferric powder in 50 mL of the same buffer. Deoxy-Mb was then generated with the addition of 5 equiv of solid sodium dithionite; the addition was carried out in a tonometer that had a Thunberg sidearm attached and, hence, permitted reduction to occur under completely anaerobic conditions. MbO_2 was generated by exposing the contents to pure O_2, and pH adjustments back to 7.6 were made with the addition of solid Tris. Solutions of MbO_2 suitable for reproducible work in the IR were always further purified at this stage by DEAE-cellulose chromatography (0.05 M Tris, 10^{-4} M EDTA, pH 8.4). The eluants were then adjusted to pH 7.6 and concentrated to 11–14 mM/L. MbO_2–MbCO conversions were achieved either by the same cyclic method used for Hb or by replacement of O_2 with CO in the dithionite reduction step.

Isolated α^{CO} and β^{CO} subunits were prepared from purified HbCO by the method of Geraci et al. (1969).

Spectral Quantitations in the Visible. Initial stock solutions, variably hydrated MIR films, and film specimens redissolved after use in MIR measurements were all routinely quantitated for the generation of ferrous and ferric species on a Cary 14 UV–visible spectrophotometer. Absolute concentrations of each species were determined by using the appropriate absorbances (630, 576, 555, and 540 nm) and their known extinction coefficients (Van Assendelft, 1970; Van Assendelft & Zijlstra, 1975) in the simultaneous equations of Benesch et al. (1973). Quantitations of intact films were made by constructing the films on the outer surface of a quartz cuvette and by establishing hydration conditions on this surface identical with those used in the MIR–IR work (see below).

IR Spectroscopy. Spectra were recorded in the double-beam absorbance mode on a Perkin-Elmer 580 grating IR spectrophotometer. The instrument was interfaced to an Interdata 6/16 computer to facilitate various spectral manipulations. Spectral references used in either manual or computer-assisted recordings of CO and oxy difference spectra consisted of the corresponding met derivative, or the opposite liganded ferrous derivative, under identically matched conditions relative to the sample. Conventional difference spectra of solution samples were obtained by using two, accurately matched, variable path-length, calcium fluoride cells (Specac P/N 7000) in the sample and reference beams. Exact matching of path lengths (26.0 ± 0.5 μm) and temperature (20 ± 1 °C) was achieved by equalizing the interference fringe patterns generated by the empty cells and by fitting both cells with thermostated jackets. The temperature was monitored inside both cells with a Bailey Instruments multichannel thermometer and two microthermocouple probes, each of which was positioned just adjacent to the beam impingement area. MIR difference spectra of solutions and variably hydrated films were obtained by using two identical Perkin-Elmer internal reflectance stages, either together in the sample and reference beams (manual operations) or separately with the aide of reference retrieval methods afforded by the computer. A vertically oriented germanium reflectance crystal (52 × 20 × 2 mm) set at a 45° angle of incidence relative to the prefocused beam (~25 internal reflections) served as the solution and film sample surface. A liquid sample holder attached to the crystal allowed for the positioning of solutions against the surface and also provided a constant humidity enclosure space directly over the films.

Difference spectra were recorded over a number of specified wavenumber ranges: 3500–2500 (ν_{OH}, ν_{NH}, ν_{CH}), 2100–1900 (ν_{CO}), and 1200–1050 cm^{-1} (ν_{O_2}). This was done in order to detect any changes that might also occur in the vibrational stretching of bulk liquid water ($\nu_{OH} \sim 3450$ cm^{-1}), amorphous (icelike) globin-bound water ($\nu_{OH} \sim 3260$–3250 cm^{-1}; $\nu_{NH} \sim 3300$ cm^{-1}), and globin –CH groups ($\nu_{CH,CH_2} \sim 3000$–2850 cm^{-1}). Any such changes might then be correlated with those pertaining only to the heme-bound ligands and their immediate environment.

Instrumental scan parameters were set as follows: resolution 3.7–2.1 cm^{-1}; scan rates 100 (ν_{CO})–50 (ν_{O_2}) cm^{-1}/min. Wavenumbers were calibrated either against a well-known water vapor line (1889.6 cm^{-1}) or against bands from polystyrene (1154.3 and 1028.0 cm^{-1}). The estimated error in ν_0 for all ν_{CO} and ν_{O_2} was ±0.5 cm^{-1} at most.

The integrated areas of fully resolved bands were determined by computer integrations and then checked by planimetry. Partially resolved bands were integrated by planimetry alone, after assuming a symmetrical peak shape about each ν_0. Base lines for each set of integrations were always established ±30 cm^{-1} relative to each ν_0.

Quantitation of Film Hydration Values. Typical MIR films were constructed on the sample face of the Ge internal reflectance crystal by first applying a thin coating of concentrated protein stock solution to the surface. A constant humidity atmosphere was then established directly over the film by first bubbling the desired gas (e.g., N_2, O_2, air, ...) through a constant humidity salt solution at a controlled rate and then passing it through the Luer ports of the liquid sample assembly block. Various levels of film hydration were then generated by making small adjustments in the flow rate of an atmosphere 98% in relative humidity.

Hydration values (g of H_2O/g of protein) were quantitated by the use of a simple film gravimetric procedure and from protein concentration values determined on redissolved films. The weight of each film at any level of hydration (W_F) was obtained directly from the weight difference between the Ge crystal plus film and the same vacuum-dried crystal minus the

film ($W_{C,F} - W_C = W_F$). The weights contributed to the film by protein alone (W_P) and any component buffer salts (W_S) were independently determined from protein concentration values obtained on an accurately determined volume of the redissolved film and from a prior knowledge of the buffer concentration. All weights were taken on a Sartorius analytical balance (±0.1 mg) immediately before and after each IR recording, and the average was used in the gravimetric expressions

$$W_F - W_P - W_S = W_{H_2O} \quad (1)$$

and

$$W_{H_2O}/W_P = \text{hydration} \quad (2)$$

The procedure yielded a reproducible set of hydration values that ranged from 1.2 to 0.1 g of H_2O/g of protein with an estimated error of ±6% or less.

Hydrogen–Deuterium Exchange in Hydrated and Dehydrated Films. H–D exchange kinetics were studied at high and low levels of film hydration, in order to (1) assess the nature and magnitude of any globin structural changes that might be associated with induced shifts in the relative populations of bound ligand species and (2) establish if the proteins undergo denaturation during film dehydration–rehydration procedures. Only a slightly modified version of the D_2O exchange procedure of Deutschmann & Ullrich (1979) was used for this purpose. The modification consisted of conducting H–D exchange on films, which in addition to being initially taken to conditions of minimal hydration (~ 0.1 g of H_2O/g of protein) were also preequilibrated to full hydration (≥1.2 g of H_2O/g of protein) with an atmosphere saturated with H_2O just before H–D exchange. Low levels of hydration were maintained in the dehydrated films, during their exposure to D_2O, by upping the flow rate of the D_2O-saturated atmosphere. These modifications allowed us to establish conditions that tended to highlight any changes in the exchange process due to dehydration alone.

CO Photodissociation and O_2 Exchange in Variably Hydrated Films. The relative ability of distinct Fe–CO modes to lose CO by photolysis or by displacement with O_2 was also examined in fully and partially hydrated films. Photolysis was carried out by exposing the films to 10-s pulses of ordinary white light for ~3-min durations; Fe–CO → Fe–O_2 exchange was achieved by exposing the films to prehumidified atmospheres of O_2 or air. Photolysis and exchange were both conducted at constant film hydration values in order to minimize the effects of hydration on Fe–CO interconversions. The decline of intensity at specific Fe–CO bands was then monitored in each case. In order to additionally verify the exchange to Fe–O_2, absorption was also monitored over 1200–1050 cm^{-1}.

The loss of O_2 from discrete Fe–O_2 signals in the oxy derivatives was similarily investigated, but only by displacement with prehumidified CO.

MIR–IR Controls. Silicon and KRS-5 crystals were used in place of Ge in several of the experiments. This was done in order to examine any artifacts that might arise from interactions between the globin surface and the MIR crystal surface.

Possible effects stemming from an expected enhancement of protein–protein packing interactions in the films were at least partially eliminated by taking spectra of films doped with 1–5-fold excesses of an intermolecular "spacer" protein; bovine serum albumin was used for this purpose.

Salt effects were examined by running spectra on films made out of either completely deionized solutions or solutions reconstituted with 1–20-fold additions of various cationic and anionic species, e.g., NH_4^+, Na^+, K^+, Mg^{2+}, Ca^{2+}, Cl^-, SO_4^{2-}, and $-OPO_3^{2-}$.

MIR spectra were also measured on HbCO and HbO_2 samples, which were constructed out of purposely denatured material. Heat (55 °C for 2–5 min followed by 0–4 °C equilibrations overnight), sodium dodecyl sulfate (0.5 M), and guanidinium chloride (6.0 M) served as the denaturants. Spectra were measured at both early (2–5 min) and late (>24 h) stages of denaturation. These studies, when combined with the H–D exchange experiments and measurements of $\Delta\nu_{1/2}$, allowed us to carefully monitor any film denaturation effects that might arise.

MIR spectra of fully hydrated and partially hydrated films of isolated α^{CO} and β^{CO} chains were recorded to examine any effects which might arise due to the breakup of the normal subunit structure in Hb.

Results

Hydration Effects on the Vibrational Stretching of Heme-Bound Ligand Conformer Modes. The general spectral features and fractional populations that we observe for discrete, rapidly interconverting, Fe–CO conformer modes in HbCO (ν_{CO} ~ *1968 cm^{-1}*, $\Delta\nu_{1/2}$ ~ 8 cm^{-1}, 1–2%; *1951 cm^{-1}*, ~8 cm^{-1}, ~98–99%) and in MbCO (ν_{CO} ~ *1967 cm^{-1}*, <1%; *1944 cm^{-1}*, ~12 cm^{-1}, 72%; *1933 cm^{-1}*, 28%) are found to be virtually identical in solution and in fully hydrated MIR films. Both kinds of spectra are also found to be in total agreement with previously reported Fe–CO spectra obtained in solution (Makinen et al., 1979; Choc & Caughey, 1981). In fact, we have found that the spectral features seen in films, for both heme-bound CO and O_2, are identical with those seen in solution, as long as the films are maintained at certain minimal hydration values for each specific combination of protein and heme ligand, i.e., 1.2 and 0.4 g of H_2O/g of protein for HbCO and MbCO, respectively, and 0.2 for HbO_2 and MbO_2. This makes it highly unlikely that the film environment alone causes any of the subsequently observed spectral changes. Indeed, it instead almost immediately hints of the presence of globin-dependent and ligand-dependent differences in the dynamic effects caused by altered hydration.

The gradual removal of water from fully hydrated films results in pronounced intensity increases in the 1968- and 1967-cm^{-1} Fe–CO conformer bands in HbCO and MbCO, respectively (Figure 1b–d). These increases are accompanied by corresponding decreases in the intensity of all of the lower wavenumber conformers that normally dominate the spectra at high hydration. The hydration effects on Fe–CO intensity are found to be completely reversible in both proteins, and the 1968–1967-cm^{-1} conformer populations are readily returned to their usual trace levels by simply reexposing the films to high humidity or by the direct readdition of bulk water. If the overall increases of intensity due solely to total protein concentration increases (see Figure 1a,b) are taken into account by transforming to a mole absorption coefficient basis (see corrected lines in Figures 2 and 3), then the total integrated intensity comprising all Fe–CO modes is seen to remain constant to within ±6% in both MbCO and HbCO. The combined results therefore indicate that the removal of water ellicits a completely reversible interconversion of the conformer population toward 1968–1967 cm^{-1} and that this capacity for interconversion between Fe–CO modes exists throughout most of the range of hydration values studied.

Several interesting globin-dependent differences appear when the integrated intensity of the 1968–1967-cm^{-1} band is expressed as a fraction of the total intensity and is plotted against film hydration (Figure 4). The relative population

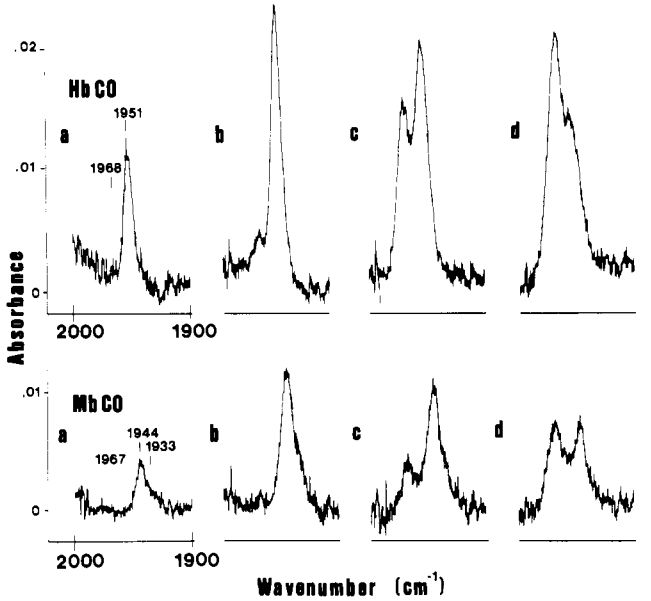

FIGURE 1: MIR–IR spectra of aqueous solutions (a) and variably hydrated films (b–d) of human HbCO and sperm whale MbCO. (a) Starting concentrations of solution samples: 3.56 mM HbCO (tetramer) and 12.32 mM MbCO. Film hydration values in grams of H_2O per gram of protein for HbCO and MbCO, respectively: (b) 0.90, 0.41, (c) 0.54, 0.24, and (d) 0.29, 0.15. The initial overall absorbance increases noted in going from (a) to (b) simply reflect the initial increases in protein concentration in going from solution to film states. They are corrected for in subsequent peak integrations. Spectra are ordinate and abscissa expanded 20 and 2 times, respectively.

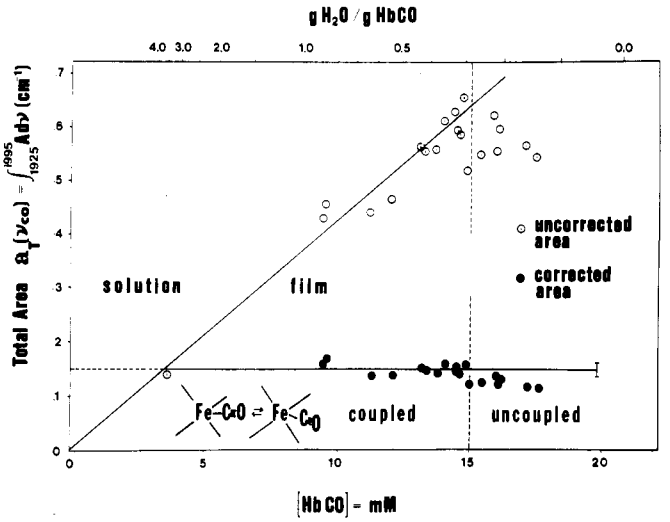

FIGURE 2: Plot showing the variation of uncorrected and corrected total integrated area for CO stretching in HbCO (sum of all Fe–CO conformer bands) as a function of film protein concentration and film hydration. Corrected areas were obtained by normalizing in each case against the area corresponding to the initial aqueous solution concentration value. The line and error bar for the corrected data points correspond to the mean corrected area for all points ≤15 mM and its estimated standard deviation, respectively. The increased scatter and deviations from constant area beyond 15 mM (or ~0.2 g of H_2O/g of HbCO) in both curves are due to uncoupling of rapid interconversions between discrete Fe–CO modes and the gradual freezing-in of independent Fe–CO conformer populations (vertical dashed line).

of this conformer is seen to increase linearly with decreasing film hydration thoughout the entire range of values studied in HbCO. A major shift toward it does not occur in MbCO until a hydration value of 0.4 is reached; however, once this value is reached, a steeper linear rise is initiated toward 1967 cm^{-1}. Distinct differences also exist between HbCO and

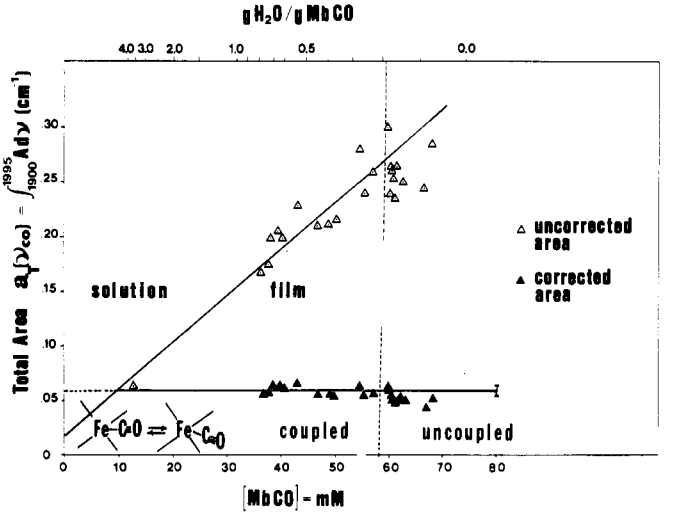

FIGURE 3: Plot showing the variation of uncorrected and corrected total integrated area for CO stretching in MbCO (sum of all Fe–CO conformer bands) as a function of film protein concentration and film hydration. Corrected areas were obtained as in Figure 2. The corrected line and error bar have the same meaning as in Figure 2, but with a cutoff of data point usage of ≤58 mM.

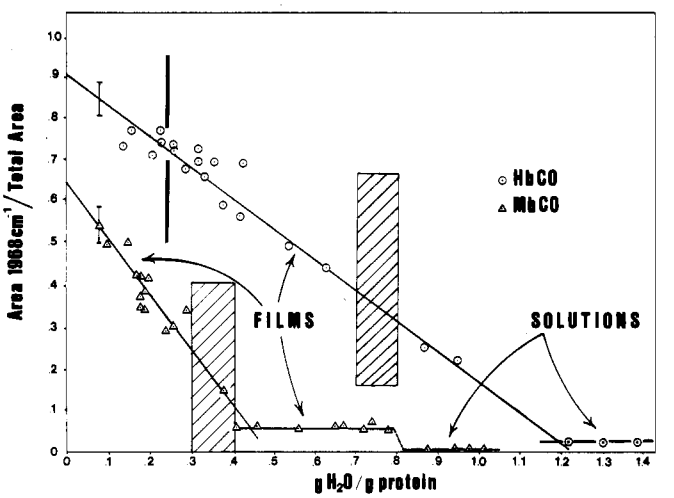

FIGURE 4: Plot showing changes in the relative population of 1968 (HbCO) and 1967 cm^{-1} (MbCO) Fe–CO conformer modes with changing film hydration. Error bars (top left) represent the estimated standard deviations of the best straight lines through linear components of the intensity shift toward 1968–1967 cm^{-1}; $|r| = 0.97$ and 0.96 for HbCO and MbCO lines, respectively. Shaded regions encompass the known hydrodynamic hydration values for HbCO and MbCO in solution (Squire & Himmel, 1979). The vertical line marks the theoretically predicted hydration value (0.24) corresponding to the first hydration monolayer for ferrous liganded Hb (Halle et al., 1981).

MbCO with respect to the maximum population eventually reached by this conformer, i.e., up to 75% of the total Fe–CO in HbCO and up to 55% in MbCO, but with each respectively corresponding to ~40–80-fold and 55–110-fold increases overall. The hydration plots also indicate that the dehydration-induced shifts correlate nicely with hydrodynamically determined values for water associated with each globin structure in solution, i.e., 0.80 g of H_2O/g of liganded Hb and 0.35 g of H_2O/g of liganded Mb (Squire & Himmel, 1979; P. G. Squire, personal communication). It is particularly interesting to note that significant shifts (~20-fold) begin to occur in HbCO at hydration values (0.9) corresponding to ~4 times that of its theoretically predicted first hydration monolayer (0.24) (Kuntz & Kauzman, 1974; Halle et al., 1981).

Maximal shifts toward 1968–1967 cm^{-1} are accompanied by minimal changes in ν_{CO} and $\Delta\nu_{1/2}$. Even extensively de-

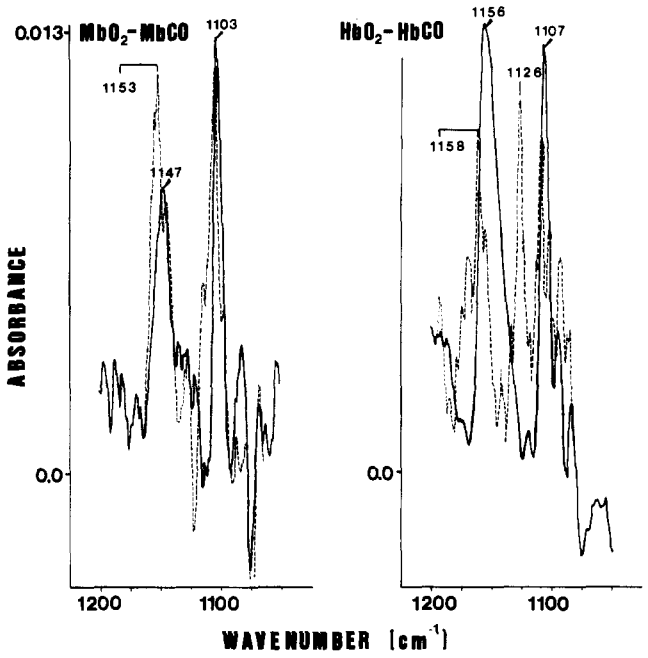

FIGURE 5: IR difference spectra of MbO_2 and HbO_2 in aqueous solution (hydration ≥ 1.2) (solid lines) and in extensively dehydrated MIR films (hydration ≤ 0.2) (superimposed dashed lines). The corresponding CO derivative was used as the reference material in each case. Concentrations used in the solution spectra were 10.37 mM MbO_2 and 3.30 mM HbO_2 (tetramer). Solution spectra consist of a 20-fold accumulation of a single difference spectrum and are abscissa and ordinate expanded by 2 and to full scale, respectively. Film spectra were simply expanded (same) and smoothed. The two absorbance scales for solution and film spectra differ and should therefore only be interpreted on a relative basis.

hydrated films show only +1 cm^{-1} shifts in ν_{CO} and 2–4-cm^{-1} increases in $\Delta\nu_{1/2}$, and both of these are exclusively associated with the intensity increases involving the 1968- and 1967-cm^{-1} bands. The absence of major band broadening effects (e.g., $\Delta\nu_{1/2} \sim 20$–25 cm^{-1}) in either the 1968–1967-cm^{-1} or the lower ν_{CO} conformers tends to rule out denaturation as a factor in the observed shifts (Yoshikawa et al., 1977; Alben, 1978; Makinen et al., 1979; Choc & Caughey, 1981). The small broadening noted at 1968–1967 cm^{-1} indicates that the stabilization of this mode may be associated with only a small gain of disorder in its immediate Fe–CO surroundings. For the most part, however, all Fe–CO configurations appear to continue to probe uniformly ordered distal surroundings within the heme pocket, irrespective of the sample state or hydration level.

In contrast to the sensitivity exhibited by Fe–CO toward the removal of water, the oxy forms show no changes in their IR spectra until hydration values of 0.2 or less are reached (Figure 5). Hence, a distinct ligand-dependent difference is seen to exist in terms of the relative ease with which Fe–CO and Fe–O_2 feel the effects of altered hydration constraints. In MbO_2, the change is limited to an extremely small range of low hydration values (~0.2–0.1) and simply consists of a sudden equalization of the heights of the Fe–O_2 stretching bands detected at 1147 and 1103 cm^{-1}. The corresponding 1156- and 1107-cm^{-1} bands in HbO_2 are already of equal peak intensity and undergo no further change relative to one another. However, at low hydration values a new band appears at 1126 cm^{-1}. Both sets of oxy spectra are computer-enhanced and are felt to represent a significant improvement over previous recordings (Barlow et al., 1973; Maxwell et al., 1974; Alben et al., 1978). Accordingly, their analysis with regard to questions concerning the actual existence of Fe–O_2 conformers and the possible complicating influence of Fermi coupling (Alben et al., 1978; Tsubaki & Yu, 1981) is dealt with in greater detail in a forthcoming paper.

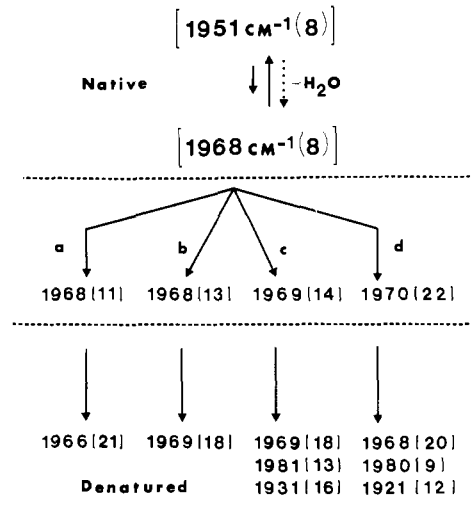

FIGURE 6: Schematic illustration of the behavior of HbCO IR spectra before and during the progression of various forms of denaturation. Numbers in brackets are the corresponding bandwidths at half-intensity ($\Delta\nu_{1/2}$) for each observed Fe–CO conformer band. The equilibrium at the top corresponds to what is seen under solution and variably hydrated film conditions. The middle and lower portions of the scheme illustrate changes seen in the early (2–5 min) and late (24-h equilibration) stages of denaturation: (a) acid–base denaturation (Choc & Caughey, 1981), (b) heat, (c) $NaDodSO_4$, and (d) guanidinium chloride.

Control Results. None of the nondenaturing control conditions specified above leads to significantly different results. Even under those conditions resulting in an overall decrease in absolute intensity (e.g., the addition of excess BSA as an intermolecular spacer), the shifts in relative intensity occur to the same extent. In addition, our preliminary results on isolated α^{CO} and β^{CO} chains indicate that they exhibit the same broad range of hydration-induced behavior as the intact HbCO tetramer.

Precursor Relationship between the 1968–1967-cm^{-1} Conformer and Various Disordered Denaturation Modes. When the progressive effects of a number of chemically distinct denaturation processes are followed in HbCO, under both MIR and conventional solution conditions, an interesting pattern of conformational changes reveals itself (Figure 6). For all of the processes followed by us (heat, $NaDodSO_4$, and guanidinium chloride) and the acid–base denaturation of HbCO followed by Choc & Caughey (1981), the early stages of denaturation are characterized by the consistent appearance of a broadened band falling in the range 1970–1968 cm^{-1} ($\Delta\nu_{1/2} \sim 13$–22 cm^{-1}). In each case, these broadened signals emerge out of the original trace population of the narrower banded 1968-1967-cm^{-1} mode. As equilibrium denaturation conditions are reached, these bands tend to undergo slight additional broadening ($\Delta\nu_{1/2} \sim 18$–20 cm^{-1}) and significant intensification, until they at least partially dominate the spectra. These later stages, in $NaDodSO_4$- and guanidinium-treated samples, also include the generation of other conformer bands that fall in the range 1981–1921 cm^{-1}. These trends not only confirm the absence of denaturation effects in the film hydration studies reported here but also reveal that the 1968–1967-cm^{-1} species is consistently predisposed toward generating any of a number of more highly disordered modes.

H–D Exchange Behavior Associated with the 1968–1967-cm^{-1} Conformer Mode. The same film conditions that lead to the large shifts toward the 1968–1967-cm^{-1} Fe–CO con-

Table I: H-D Exchange Behavior Associated with the Shift toward 1968–1967 cm^{-1} in Variably Hydrated Films of Liganded Hb and Mb

kinetically distinct classes of exchanging H[a]	fully hydrated films[b] (%)	partially dehydrated films[c] (%)	estimate from X-ray structures[d] (%)	denatured controls[e] (%)
Hb-L				
fast (0–3 min)	17	21	17	55
intermediate (10–40 min)	14	20	15	
slow (40–120 min)	70	60	68	
Mb-L				
fast (0–3 min)	17	22	23	66
intermediate (10–40 min)	18	16	11	
slow (40–120 min)	65	62	66	

[a] Determined from straight line components of log ($A_{NH\ II}/A_{NH\ I}$) vs. T_X plots by extrapolation (Deutschmann & Ullrich, 1979). [b] 1968–1967-cm^{-1} mode at minimal (0.5–2%) relative population. [c] 1968–1967 cm^{-1} mode at maximal (55–75%) relative population. [d] Fast exchanging H estimated from fully exposed, non-H-bonded, peptide groups. Intermediate exchanging H estimated from solvent-inaccessible, non-H-bonded peptides, 3_{10} helices, and irregular helical segments. Slow exchanging H estimated from remaining pure α-helical segments containing intact H-bonded peptides. [e] Films constructed out of material exposed to 55–80 °C water bath heat for 2–5 min.

Table II: Comparison of Deoxy-like Visible Spectra Changes Accompanying the Shift toward 1968–1967 cm^{-1} with Those Accompanying the Buildup of Proximal Steric Hindrance in Model Heme Complexes

sample	visible absorption λ_{max} (nm)					band intensity ratios		
	α		555 min		β	α/β	α/555 min	β/555 min
proteins								
MbCO (soln)	579	(blue)	561	(blue)	542	0.88	1.24	1.40
MbCO (film)[a]	574		559		541	0.89	1.09	1.25
HbCO (soln)	569	(red)	555	(red)	539	1.00	1.27	1.27
HbCO (film)[a]	570		557		540	0.96	1.10	1.15
MbO_2 (soln)	581	(blue)	563		543	1.03	1.81	1.78
MbO_2 (film)[a]	580		563		543	0.95	1.48	1.55
HbO_2 (soln)	577	(red)	560	(red)	541	1.06	1.82	1.70
HbO_2 (film)[a]	578		562		543	0.99	1.25	1.27
protoheme complexes[b]								
CO:1-BI[c]	569	(blue)	555	(blue)	539	0.92	1.14	1.22
CO:1,2-DMI[d]	564		551		538	0.99	1.04	1.05
O_2:1-BI[c]	574	(red)	560	(red)	540	0.99	1.71	1.74
O_2:1,2-DMI[d]	576		565		544	0.81	1.14	1.41

[a] Film samples at hydration levels causing either a maximal shift toward 1968–1967 cm^{-1} in the CO derivatives or a maximum change in the Fe–O_2 spectra of the oxy forms. [b] Distal:proximal ligands. [c] 1-Butylimidazole (unhindered) (Wang & Brinigar, 1979). [d] 1,2-Dimethylimidazole (hindered proximally) (Wang & Brinigar, 1979).

former also lead to H–D exchange behavior that is consistent with only a slight disordering or expansion of the globin structure (Table I). The liganded forms of both Hb and Mb show 4–5% increases in fast exchanging protons (0–3 min) and 3–10% decreases in slow exchanging protons (40–120 min), following the establishment of low hydration levels equivalent to those giving maximal populations of the 1968–1967-cm^{-1} species. Hb also exhibits a 6% increase in intermediate exchanging protons (10–40 min). The range of percentages for fast exchanging protons for both proteins at either of the film hydration extremes is also determined to be far below that of corresponding heat-denatured control materials, i.e., 17–22% vs. 55–66% within a 3-min exposure to D_2O. In addition, the denatured controls rapidly lose all evidence for the continued existence of three or more kinetically distinct classes of exchanging protons. The films do not.

Correlations between the Shift toward 1968–1967 cm^{-1} and the Buildup of Deoxy-like Steric Constraints Proximal to the Heme. Changes in the visible spectra accompanying those seen in the IR are compared in Table II. The most significant change consistently seen in both the CO and oxy forms of the proteins is a rise in visible absorption intensity at 555 nm. This deoxy-like intensity enhancement occurs at hydration values identical with those leading to maximal shifts toward 1968–1967 cm^{-1} and to the more subtle oxy IR changes. It also disappears in the same highly reversible fashion upon rehydration of the films. An additional comparison of α/555 and β/555 band intensity ratios for the effect seen in the films and for changes attributed to the build up of deoxy-like proximal steric hindrance in imidazole-substituted CO and O_2 protoheme complexes (Table II; Wang & Brinigar, 1979) also illustrates that enhanced absorption at 555 nm is characteristic of a shift toward such a steric buildup. Thus, for both effects, α/555 and β/555 exhibit similarly sized decreases (555-nm increases) and the same order for such decreases between CO and O_2 derivatives, i.e., O_2 > CO.

Other changes seen in the visible not only suggest a shift toward enhanced steric constraints proximal to the heme, they also underscore the existence of subtle globin- and ligand-dependent differences in the nature of this shift. Thus, the increase at 555 nm in MbCO is accompanied by 1–5-nm blue shifts in the α and β bands and by a slight increase in the α/β ratio; in HbCO, it is accompanied by small red shifts and a significant decrease in this ratio. MbCO therefore illustrates dehydration-induced changes in the visible that exactly parallel those associated with the enhancement of deoxy-like proximal steric effects in model heme complexes, while HbCO shows a small reversal in this trend. However, when the same kind of comparison is made between the oxy derivatives, it is HbO_2 which then exhibits a strong parallel trend. Under no circumstances do we detect the actual presence of deoxy-Hb or deoxy-Mb in the films. We can therefore state unequivocally that the adoption of these deoxy-like changes occurs while CO and O_2 still occupy the sixth coordination site at the hemes and that they are not induced by packing interactions involving the deoxy forms of the proteins (Makinen et al., 1979).

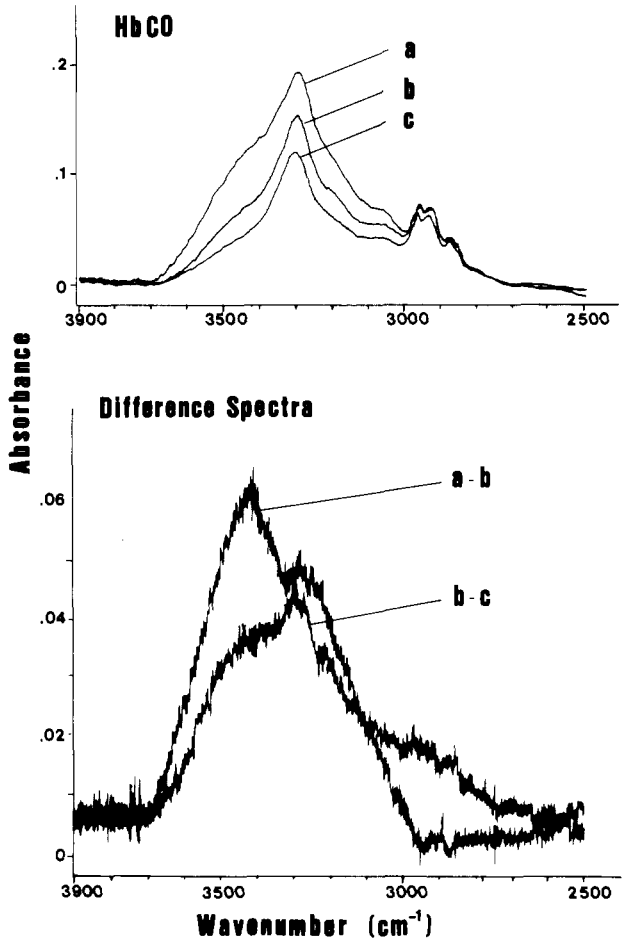

FIGURE 7: MIR–IR spectra (top) and corresponding difference spectra (bottom) of a HbCO film in the water OH, peptide NH, and globin CH stretching regions. Spectral tracings a–c encompass the same range of hydration values that were used to generate shifts in the Fe–CO conformer equilibria toward 1968 cm^{-1} (see text). Film hydration values (in g of H_2O/g of HbCO) were (a) 1.00, (b) 0.30, and (c) 0.20.

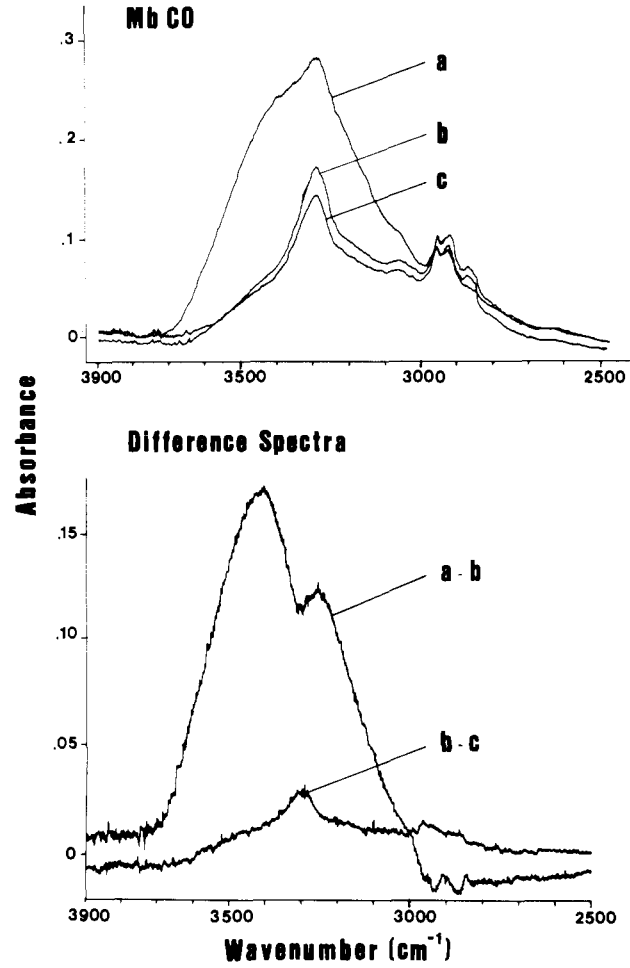

FIGURE 8: MIR–IR spectra (top) and corresponding difference spectra (bottom) of a MbCO film in the water OH, peptide NH, and globin CH stretching regions. Spectral tracings a–c encompass the same range of hydration values that were used to generate shifts toward the 1967-cm^{-1} Fe–CO species (see text). Film hydration values (in g of H_2O/g of MbCO) were (a) 1.20, (b) 0.20, and (c) 0.1.

Corresponding Decreases in Liquid and Amorphous Icelike Water OH Stretching. Changes occurring in the 3500–2800-cm^{-1} region of the IR spectra are shown in Figures 7 and 8. The sequence of absorption profiles, a–c, and the corresponding sets of difference spectra, a – b and b – c, shown in each figure closely match the film hydration conditions that were used in Figure 1b–d; they should therefore reflect any changes in bulk liquid and structured water that accompany the observed Fe–CO conformer shifts in HbCO and MbCO.

When the films are taken from the fully hydrated state (a; ~1.0) to hydration levels leading to a major shift toward 1968–1967 cm^{-1} (b; ~0.3–0.2), the greatest accompanying change is seen to be an intensity decrease at 3450 cm^{-1}. Somewhat smaller decreases also occur throughout the unresolved system of bands falling in the range 3300–3000 cm^{-1}. In the difference spectra (a – b), this shows up as a larger positive difference peak at 3450 cm^{-1} followed by a smaller partially resolved shoulder falling at 3000–3250 cm^{-1}. As the films are taken to hydration values that maximize the population of 1968–1967-cm^{-1} species (c; ~0.2–0.1), this pattern tends to reverse; either slightly smaller or no further decreases occur at 3450 cm^{-1} along with the continuation of decreases at 3300–3000 cm^{-1} (b – c). Throughout the entire range of hydration changes, the intensities of discrete CH modes are seen to change only slightly.

The broad shoulder absorption centered at 3450 cm^{-1} is a well-known feature in the IR of hydrated proteins and can immediately be assigned to OH stretching on the part of bulk liquid water. Although the 3300–3000-cm^{-1} region is contributed to significantly by globin NH stretching, it has also been shown to be sensitive to changes involving an amorphous, icelike, form of globin-bound water (Buontempo et al., 1972); absorption at 3260–3250 cm^{-1}, in particular, is believed to be due to OH stretching on the part of this form of water, and both it and the 3300-cm^{-1} NH signal have been shown to diminish, rather than increase, upon its removal. Our results therefore indicate that the removal of both kinds of water accompanies the observed Fe–CO conformer shifts. In HbCO, this is true for both the initial and final stages of the shift toward the 1968-cm^{-1} species. In MbCO, the final stages of the shift toward the 1967-cm^{-1} conformer (~0.2–0.1 hydration) appear to be predominantly accompanied by the removal of the more highly structured bound form of water.

Uncoupling of Fe–CO Conformer Interconversions at Low Hydration: Unmasking of Preferential Reaction Tendencies in Specific Conformer Types. When films of either CO derivative are taken to hydration values of 0.3–0.2 or less, the discrete forms of Fe–CO begin to show a greatly diminished capacity to rapidly interconvert. Eventually, a state of dehydration is reached in the films which results in the "freezing-in" of independent populations of the various Fe–CO modes and, hence, in the complete uncoupling of conformational relaxation events (see Figures 2 and 3). At this point, the individual reaction tendencies of specific Fe–CO modes

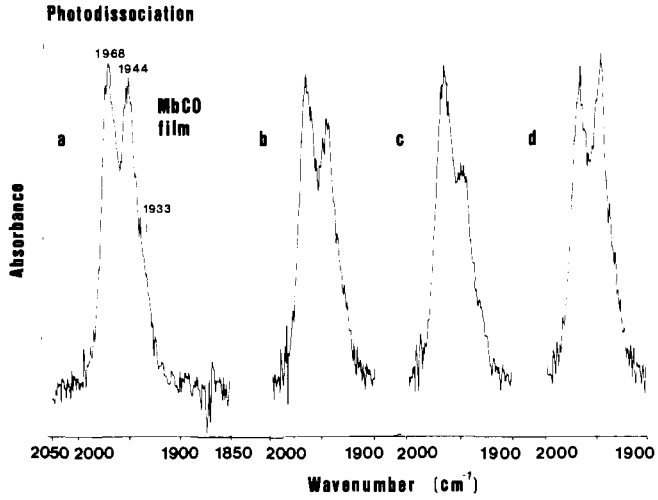

FIGURE 9: MIR–IR spectra of a MbCO film at a fixed hydration value of 0.15 g of H_2O/g of MbCO. The sequence of spectra a–c shows the preferred photodissociation tendencies (or O_2 displacement–exchange tendencies; same, but not shown) of the lower wavenumber Fe–CO conformer modes and the absence of photodissociation at 1968 cm^{-1}. Spectrum d shows the selective reestablishment of intensity at the lower wavenumber modes with the readdition of CO. Similar sets of results were obtained with HbCO films held fixed at low hydration, i.e., preferred intensity losses and losses regained at 1951 cm^{-1} with no change at 1968 cm^{-1}.

are freed from rapid equilibrium and conformer interconversion effects and can be studied on an independent basis. At the same time, the populations of 1968–1967-cm^{-1} species are raised to levels where they can now be conveniently monitored.

The spectral changes monitored in Figure 9 represent an example of how we have begun to use this state to investigate the dissociation and exchange properties of individual Fe–CO conformers in the absence of interconversion effects. Thus, spectra obtained before and after exposure of the uncoupled Fe–CO populations to light (or prehumidified O_2; not shown) reveal that the lower wavenumber Fe–CO conformers selectively diminish in intensity upon conversion to deoxy-Fe(II) (or Fe–O_2). The maximized population of 1968–1967-cm^{-1} species, on the other hand, shows very little change of intensity even after extensive exposure to these agents. In addition, there is no observable reestablishment of intensity in the lower wavenumber species following the elimination of light or O_2; however, these bands do selectively regain their lost intensity after the films are reexposed to CO (Figure 9c,d). The 1968–1967-cm^{-1} conformer consistently stays at the same maximal intensity in this state regardless of whether it is exposed to light, O_2, or additional CO. These observations therefore suggest (1) that the 1968–1967-cm^{-1} mode apparently corresponds to a more tightly bound form of CO, (2) that both CO and O_2 are able to enter and leave the heme pockets of the lower wavenumber modes, (3) that both ligands are also able to diffuse into and out of the films in the uncoupled state, and (4) that the loss of intensity at lower wavenumbers is real and does not simply result from an interconversion of the total Fe–CO population back toward 1968–1967 cm^{-1}.

At film hydration levels that allow for the restoration of Fe–CO conformer interconversions (0.3 or greater), it is much more difficult to detect any apparent differences in Fe–CO reactivity. Under such conditions, the recoupling of conformational relaxation events and the return of rapid equilibrium processes tend to disguise such differences by driving all of the unreacted Fe–CO species back to their initial equilibrium population ratios. Intensity decreases then tend to be seen at all bands during dissociation or exchange. Another difficulty in making measurements under these conditions arises due to the greatly diminished size of the 1968–1967-cm^{-1} band area. Both effects therefore make it very difficult to measure any selective trends in the redistribution of intensity between the fully coupled Fe–CO forms. However, Shimada et al. (1979) have presented evidence that indicates that the 1968–1967-cm^{-1} species would probably still correspond to a less reactive mode, even under normal fully hydrated conditions.

In contrast to heme-bound CO, we have so far been unable to detect a similar trend for preferred reactivity on the part of discrete Fe–O_2 species seen in either oxy derivative, regardless of the degree of hydration.

Discussion

The present results show that the dynamic behavior of the liganded heme and its immediate surroundings in HbCO and MbCO is surprisingly sensitive to the level of globin hydration. This is especially true when hydration changes are made to occur under close-packed conditions in films. Even the limited removal of liquid and icelike hydration constraints from a film is capable of causing 40–100-fold shifts in the relative populations of discrete Fe–CO conformer modes toward 1968–1967 cm^{-1}. In comparison, previous IR studies of pH effects, temperature effects, diminished distal steric effects due to mutationally induced changes within the heme pocket (in HbCO solutions), and altered packing effects induced in MbCO crystals (all under nondenaturing conditions) have never shown more than ~3–6-fold shifts toward this species (Caughey et al., 1978; Makinen et al., 1979; Choc & Caughey, 1981). The dynamic shifts observed in films initially occur at hydration levels that roughly coincide with the known maximum extent of globin hydration in each protein, i.e., at Hb and Mb hydration values determined by hydrodynamic methods in dilute aqueous solution (Squire & Himmel, 1979). They also only begin to become significant at film protein concentration levels (~40–60 g %) which are similar to Hb concentrations inside the red cell (~35–40 g %).

The controls used in this study and the reversibility of the dehydration–rehydration-induced shifts virtually eliminate denaturation and a number of other processes as the driving forces behind the shifts. The shifts also occur in the absence of any build up of deoxy- or met-Hb (or Mb). Thus, unlike Makinen et al. (1979), we cannot attribute the enhanced population of 1968–1967-cm^{-1} species or its association with proximal deoxy-like steric character to induced packing interactions between differentially liganded forms of the proteins. The similarity of the results obtained with BSA-doped films also argues that specific protein–protein interactions do not contribute directly to the shifts. It seems likely, however, that the enhancement of nonspecific protein–protein interactions between liganded forms of the proteins, does contribute both to the observed shifts and to the eventual uncoupling of rapid conformer interconversions. Regardless of the exact mechanism, the transmission of such effects to the hemes must involve the disruption (or, conversely, the reversible restoration) of constraints afforded by water (e.g., its hydrogen-bonding interactions with polar surface residues, its partial clathrate interactions with nonpolar surface residues, or both). This in turn must lead to the reversible stabilization and destabilization of dynamic modes that are normally available to the globin structure and, hence, normally capable of being probed by at least some heme-bound ligands.

Importance of Distal Steric Effects and Their Dynamic Coupling with Hydration Effects. The question of whether steric interactions between heme ligands and the distal surface

of the heme pocket can exert a significant discriminatory effect on the association–dissociation properties of linear vs. bent end-on ligands (Fe–CO vs. Fe–O_2) has been a matter of ongoing dispute (Collman et al., 1976, 1981; Moffat et al., 1979; Busch et al., 1981; Traylor et al., 1981; Ward et al., 1981). Our results not only illustrate the intrinsic importance of selective distal effects in Hb and Mb but also show that such effects can be significantly influenced from a dynamic standpoint by the level of globin hydration. The results show, on the one hand, that the discrete Fe–CO modes generated by the steric effects display differing abilities to undergo photolysis or O_2 exchange and, on the other, that their relative populations can be dramatically shifted by altered hydration. Consequently, their combined influence can result in a large change of reactivity in the total Fe–CO population. The fact that we have so far only been able to detect such effects in the case of a ligand that normally prefers to adopt a linear configuration relative to the heme (CO) therefore reaffirms the importance of the discriminatory topographical properties of the distal heme environment.

In light of this, it is interesting to contemplate the adverse consequences of diminished hydration or, perhaps more appropriately, the beneficial consequences of its presence. It is clear from our results that open distal heme pocket modes corresponding to the 1968–1967-cm^{-1} species would at least partially dominate the dynamics of Hb and Mb in the absence of hydration constraints. We have also seen that this mode would preferentially accommodate a less reactive form of CO. It is therefore doubtful whether either Hb or Mb would serve to function as efficient O_2 transport or storage systems under such conditions, especially in the presence of even trace quantities of CO. The hydration constraints can therefore be viewed as favoring heme pocket configurations that selectively facilitate both the dissociation of CO and association of O_2, i.e., by destabilizing the 1968–1967-cm^{-1} mode and stabilizing modes that promote tilted or bent end-on ligand configurations, which in the case of Fe-CO, evidently results in more readily dissociated forms of CO [see also Shimada et al. (1979)]. The ligand-dependent differences we see therefore indicate that hydration exerts a crucial stabilizing effect on the correct form of structural and dynamic discrimination within the heme pocket.

Significance of the 1968–1967-cm^{-1} Mode in the Dynamics of Ligand Entry–Release Processes. Choc & Caughey (1981) have recently suggested that this conformer may be probing an available globin relaxation mode that is structurally better suited to permit the entry and release of heme ligands. Their suggestion is made especially attractive by (1) the absence of any obvious sterically free pathway for ligand movements into or out of the static atomic models of the unliganded and liganded forms of either protein (Case & Karplus, 1979), (2) the consistent presence of this conformer in practically all native samples and species of HbCO and MbCO (Caughey et al., 1978), and (3) its consistent association with structural and spectroscopic properties in both normal and mutant forms (Tucker et al., 1978; Makinen et al., 1979; Choc & Caughey, 1981), which suggest that it possesses less hindered or slightly expanded distal surroundings in comparison to the dominant tilted or bent Fe–CO modes at lower ν_{CO}.

Although our results go a long way toward confirming the increased openness of this mode, they also indicate that it may not be of general importance in actually facilitating ligand entry–release, i.e., for ligands in general, O_2 in particular, or even for all of the dynamic processes involved in entry–release (entry, association, dissociation, and release). The strong correlation seen to exist between this mode and diminished hydration, while attractive in terms of its potentially affording lower surface energy barriers for entry–release processes in general, has its importance detracted somewhat by the fact that the fully hydrated constrained modes also readily permit the entry and release of CO and O_2 (see Results; Figure 9). Also, for CO specifically, any apparent advantages would appear to be largely overridden by the fact that this mode also correlates with much tighter binding on the part of CO. We would therefore tentatively limit the significance of the 1968–1967-cm^{-1} mode, in terms of any role it plays in entry–release dynamics, to a possible facilitation of CO entry and CO association events. It does not appear to contribute in any obvious way to the dissociation and release of CO.

Significance of the 1968–1967-cm^{-1} Conformer Mode in Terms of Globin Folding Dynamics. In addition to its potential significance as a ligand entry–association mode, the 1968–1967-cm^{-1} conformer exhibits properties that suggest an important linkage with globin folding pathways. The fact that it consistently exhibits an immediate precursor relationship with a number of more highly disordered conformer modes, which can only be generated by a variety of chemically distinct denaturation processes (Figure 6), indicates that it may correspond to a native folding nucleus or folding intermediate. Its already slightly expanded structure relative to the dominant native modes with which it rapidly interconverts also makes us suspect it may serve as a common starting point for unfolding events.

Acknowledgments

We thank Deirdre S. Gallagher for her expert typing of the manuscript.

Registry No. Oxyhemoglobin A, 9062-91-3; carbonylhemoglobin A, 9072-24-6; heme, 14875-96-8.

References

Alben, J. O. (1978) in *The Porphyrins* (Dolphin, D., Ed.) Vol. III, pp 323–345, Academic Press, New York.

Alben, J. O., Bare, G. H., & Moh, P. P. (1978) in *Biochemical and Clinical Aspects of Hemoglobin Abnormalities* (Caughey, W. S., Ed.) pp 607–617, Academic Press, New York.

Austin, R. H., Beeson, K. W., Eisenstein, L., Frauenfelder, H., & Gunsalus, I. C. (1975) *Biochemistry 14*, 5355–5373.

Barlow, C. H., Maxwell, J. C., Wallace, W. J., & Caughey, W. S. (1973) *Biochem. Biophys. Res. Commun. 55*, 91–95.

Benesch, R. E., Benesch, R., & Yung, S. (1973) *Anal. Biochem. 55*, 245–248.

Buontempo, U., Careri, G., & Fasella, P. (1972) *Biopolymers 11*, 519–521.

Busch, D. H., Zimmer, L. L., Grzybouski, J. J., Olszanski, D. J., Jackels, S. C., Callahan, R. C., & Christoph, G. G. (1981) *Proc. Natl. Acad. Sci. U.S.A. 78*, 5919–5923.

Case, D. A., & Karplus, M. (1978) *J. Mol. Biol. 123*, 697–701.

Case, D. A., & Karplus, M. (1979) *J. Mol. Biol. 132*, 343–368.

Caughey, W. S., Houtchens, R. A., Lanir, A., Maxwell, J. C., & Charache, S. (1978) in *Biochemical and Clinical Aspects of Hemoglobin Abnormalities* (Caughey, W. S., Ed.) pp 29–56, Academic Press, New York.

Choc, M. G., & Caughey, W. S. (1981) *J. Biol. Chem. 256*, 1831–1838.

Collman, J. P., Brauman, J. I., Halbert, T. R., & Suslick, K. S. (1976) *Proc. Natl. Acad. Sci. U.S.A. 73*, 3333–3337.

Collman, J. P., Brauman, J. I., Collins, T. J., Iverson, B., & Sessler, J. L. (1981) *J. Am. Chem. Soc. 103*, 2450–2452.

Deutschmann, G., & Ullrich, V. (1979) *Anal. Biochem. 94*, 6–14.
Geraci, G., Parkhurst, L. J., & Gibson, Q. H. (1969) *J. Biol. Chem. 244*, 4664.
Halle, B., Anderson, T., Forsen, S., & Lindman, B. (1981) *J. Am. Chem. Soc. 103*, 500–508.
Kuntz, I. D., Jr., & Kauzman, W. (1974) *Adv. Protein Chem. 28*, 239–345.
Makinen, M. W., Houtchens, R. A., & Caughey, W. S. (1979) *Proc. Natl. Acad. Sci. U.S.A. 76*, 6042–6046.
Maxwell, J. C., Volpe, J. A., Barlow, C. H., & Caughey, W. S. (1974) *Biochem. Biophys. Res. Commun. 58*, 166–171.
Moffat, K., Deatherage, J. F., & Seybert, D. W. (1979) *Science (Washington, D.C.) 206*, 1035–1042.
Rossi Fanelli, A., Antonini, E., & Caputo, A. (1961) *J. Biol. Chem. 236*, 391.
Shimada, H., Iizuka, T., Ueno, R., & Ishimura, Y. (1979) *FEBS Lett. 98*, 290–294.
Squire, P. G., & Himmel, M. E. (1979) *Arch. Biochem. Biophys. 196*, 165–177.
Traylor, T. G., Mitchell, M. J., Tsuchiya, S., Campbell, D. H., Stynes, D. V., & Koga, N. (1981) *J. Am. Chem. Soc. 103*, 5234–5236.
Tsubaki, M., & Yu, N. (1981) *Proc. Natl. Acad. Sci. U.S.A. 78*, 3581.
Tucker, P. W., Phillips, S. E. V., Perutz, M. F., Houtchens, R. A., & Caughey, W. S. (1978) in *Biochemical and Clinical Aspects of Hemoglobin Abnormalities* (Caughey, W. S., Ed.) pp 1–15, Academic Press, New York.
Van Assendelft, O. W. (1970) in *Spectrophotometry of Haemoglobin Derivatives*, Royal Van Gorcum, Ltd., Assen, The Netherlands.
Van Assendelft, O. W., & Zijlstra, W. G. (1975) *Anal. Biochem. 69*, 43–48.
Wang, C. M., & Brinigar, W. S. (1979) *Biochemistry 18*, 4960–4977.
Ward, B., Wang, C. B., & Chang, C. K. (1981) *J. Am. Chem. Soc. 103*, 5236–5238.
Yoshikawa, S., Choc, M. G., O'Toole, M. C., & Caughey, W. S. (1977) *J. Biol. Chem. 252*, 5498–5508.

Chlorophyllide-Substituted Hemoglobin Tetramers and Hybrids: Preparation, Characterization, and Energy Transfer†

Atsuo Kuki and Steven G. Boxer*

ABSTRACT: Three chlorophyllide-substituted human hemoglobin (Hb) complexes have been prepared: the tetrameric complex in which zinc pyrochlorophyllide *a* (ZnPChl*a*) is substituted for all four hemes and the two complementary hybrids in which ZnPChl*a* is substituted for heme in either the α- or β-chains, while heme remains in the other chains. In each of these complexes, intramolecular Chl–Chl singlet energy transfer occurs. A variety of probes demonstrate that ZnPChl*a*–deoxyheme hybrids and the ZnPChl*a*–Hb complexes consistently exhibit properties associated with the well-known T-state tertiary and quaternary structure of deoxyHb itself. Using the known crystal structure of human deoxyHb, we have analyzed the steady-state fluorescence anisotropy of these complexes within the framework of the Förster energy-transfer theory. The result is the determination of the orientation of the Q_y transition dipole moment of ZnPChl*a*. Nuclear magnetic resonance data for the hybrids offer insight into specific tertiary structural changes in the heme pocket surrounding the diamagnetic ZnPChl*a*, which accompany changes in the ligation state of the heme on the opposite chain.

The chlorophyll molecule in nature displays its most important electronic features in structured association with other key components of photosynthetic assemblies. As the intermolecular electronic couplings important in both energy and electron transfer are expected to be highly distance- and orientation-dependent (Förster, 1965; Jortner, 1980), the structure of the molecular assembly undoubtedly exerts control over the fate of the singlet excited state. The existence of a high level of structure has been clearly demonstrated both in bacterial reaction centers [by optical (Rafferty & Clayton, 1979) and magnetic (Boxer & Roelofs, 1979; Thurnauer & Norris, 1976, 1977; Frank et al., 1979) polarization experiments] and in a bacteriochlorophyll-containing light-harvesting antenna complex, whose crystal structure has been determined at high resolution (Matthews & Fenna, 1980). For this reason, it is most appropriate to explore the photophysical and photochemical consequences of specific interchromophore geometries and to test these concepts by the synthesis of model systems.

In response to this challenge, a number of porphyrin and chlorophyll dimers and higher oligomers have been synthesized and characterized in which the structure is defined by specific hydrogen bonding, covalent linkage, and interchromophore π–π association [see Bucks & Boxer (1982) for a review]. In all cases investigated to date, the chlorophylls are in or near to van der Waals contact; consequently, the electron–electron Coulombic repulsion is predicted and observed to produce a strong excitonic interaction (Kasha et al., 1965), and the finite orbital overlap allows the possibility of rapid electron transfer (Netzel et al., 1982).

In this paper we report the synthesis, characterization, and steady-state emission properties of chlorophyll dimers of a completely different sort, possessing interchromophore distances of 25–40 Å. By specific insertion of zinc pyrochlorophyllide *a* (ZnPChl*a*)[1] (Figure 1) into the heme pockets

† From the Department of Chemistry, Stanford University, Stanford, California 94305. *Received December 20, 1982.* This work was supported by grants from the National Science Foundation (PCM-7926677) and the U.S. Department of Energy (DE-FG02-80-CS84006). The 360-MHz NMR spectra were obtained at the Stanford Magnetic Resonance Laboratory, supported by National Science Foundation and National Institutes of Health Grants GR23633 and RR00711, respectively. S.G.B. is an Alfred P. Sloan and Camille and Henry Dreyfus Teacher-Scholar Fellow.

0006-2960/83/0422-2923$01.50/0